7

Response of Continuous Pipelines To Transverse PGD

As mentioned previously, transverse PGD refers to permanent ground movement perpendicular to the pipe axis. When subject to transverse PGD, a continuous pipeline will stretch and bend as it attempts to accommodate the transverse ground movement. The failure mode for the pipe depends then upon the relative amount of axial tension (stretching due to arc length effects) and flexural (bending) strain. That is, if the axial tension strain is low, the pipe wall may buckle in compression due to excessive bending. On the other hand, if axial tension is not small, the pipe may rupture in tension due to the combined effects of axial tension and flexure. T. O'Rourke and Tawfik (1983) present a case history, from the 1971 San Fernando event, of continuous pipe failure due to PGD. The transverse component of PGD was approximately 1.7 m. Line 1001 (Pipeline 5 in Figure 2.11 (a)) was abandoned because of multiple breaks. Line 85 (Pipeline 4 in Figure 2.11(a)) was repaired at several locations within the PGD zone. The records indicate that three repairs near the eastern boundary of the soil movement were due to tensile failure and two other repairs near the western boundary were due to compressive failure. Note that besides the major lateral movement, there was small axial movement toward the west.

Similar to longitudinal PGD, pipeline response to transverse PGD is in general a function of the amount of PGD δ, the width of the PGD zone as well as the pattern of ground deformation. Figure 7.1 presents sketches of two types of transverse patterns considered herein.

Observed examples of **spatially distributed** transverse PGD (sketched in Figure 7.1(a)) have previously been presented in Figure 2.11(b) and (c) and in Figure 2.11(a) near Pipeline 2. In these cases, the pipe strain is a function of both the amount and width of the PGD zone. Observed examples of **abrupt** transverse PGD (sketched in Figure 7.1(b)) have previously been presented in Figure 2.11(a) near Pipelines 4 and 5. In these cases, the pipe strain is

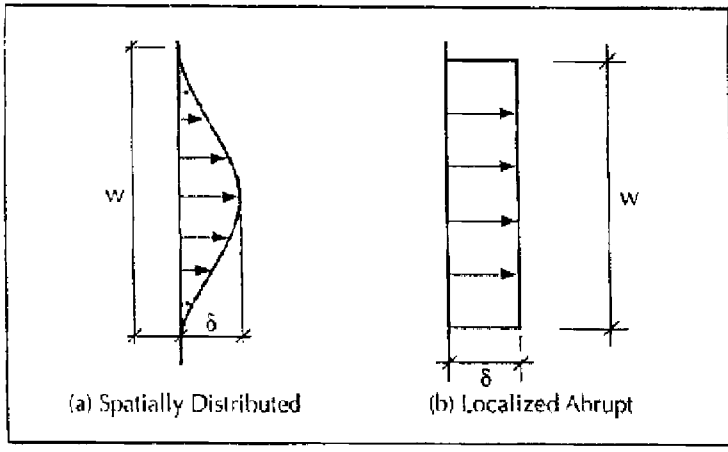

■ Figure 7.1 Patterns of Transverse PGD

a function of δ and in some cases, the width of the zone *W*. That is, if the zone is wide, the movement at each margin of the PGD zone corresponds more or less to a fault offset where the fault/pipeline intersection angle is 90°.

Another type of transverse PGD occurs when a pipe is buried directly in liquefied soil. In addition to the pipe deformation in the horizontal direction due to lateral spreading of liquefied soil, it may also uplift due to buoyancy (transverse deformation in the vertical direction). This mechanism has caused pipe damage in past events. For example, Suzuki (1988) and Takada (1991) mentioned that some pipes, with or without manholes, were uplifted out of the ground due to buoyancy effects during the 1964 Niigata earthquake.

In this chapter, we discuss continuous pipeline response to spatially distributed transverse PGD in detail. Various analytical idealizations of transverse PGD which have been used are reviewed. Analytical and numerical models of pipe response to spatially distributed transverse PGD are then discussed. The cases of a pipeline in a competent soil layer and in a liquefied layer are presented separately. Also, the effects of the buoyance force are discussed. Finally, the conditions whereby abrupt transverse PGD may be modeled as a special case of fault offset are presented. The topic of pipe response to fault offset is discussed in Chapter 8.

7.1

IDEALIZATION OF SPATIALLY DISTRIBUTED TRANSVERSE PGD

One of the first items needed to evaluate pipeline response to spatially distributed transverse PGD is the pattern of ground deformation, that is, the variation of ground displacement across the width of the PGD zone. Different researchers have used different patterns in their analyses.

T. O'Rourke (1988) approximates the soil deformation with the beta probability density function,

$$y(x) = \delta[s/s_m]^{r'-1}[(1-s)/(1-s_m)]^{\tau-r'-1} \quad 0 < s < 1 \qquad (7.1)$$

where s is the distance between the two margins of the PGD zone normalized by the width W, s_m is the normalized distance from the margin of the PGD zone to the location of the peak transverse ground displacement, δ, while r' and τ are parameters of the distribution. In his analysis, the following values were used; $s_m = 0.5$, $r' = 2.5$ and $\tau = 5.0$. Figure 7.2 shows the resulting idealized soil deformation.

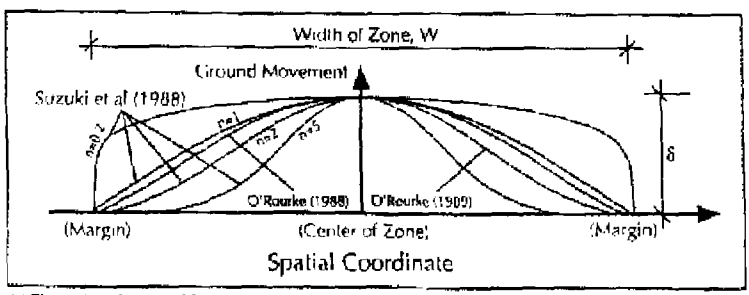

■ Figure 7.2 Assumed Patterns for Spatially Distributed Transverse PGD

Suzuki et al. (1988) and Kobayashi et al. (1989) approximate the transverse soil deformation by a cosine function raised to a power n.

$$y(x) = \delta \cdot \left(\cos \frac{\pi x}{W} \right)^n \qquad (7.2)$$

where the non-normalized distance x is measured from the center of the PGD zone. Figure 7.2 also shows the Suzuki et al. and Kobayashi et al. model for n = 0.2, 1.0, 2.0 and 5.0.

M. O'Rourke (1989) assumes the following function for spatially distributed transverse PGD:

$$y(x) = \frac{\delta}{2} \left(1 - \cos \frac{2\pi x}{W} \right) \qquad (7.3)$$

where x is the non-normalized distance from the margin of the PGD zone. This gives the same shape as both the Suzuki and Kobayashi et al.'s models with n = 2.0 (note, origin of x axis is shifted).

As shown in Figure 7.2, all the patterns are similar in that the maximum soil deformation occurs at the center of the PGD zone and the soil deformation at the margins is zero. The patterns differ in the variation of ground deformation between the center and the margins.

7.2 PIPELINE SURROUNDED BY NON-LIQUEFIED SOIL

Pipelines are typically buried about 1.0 m (3 ft) below the ground surface. Often the ground water level and the top surface of the liquefied soil layer are both below the bottom of the pipe. In these cases the force-deformation relations at the soil-pipeline interface correspond to a pipe in competent non-liquefied soil which overrides a liquefied soil layer.

In the following subsections, results from various analytical approaches and nonlinear finite element approaches will be presented and compared. Results for pipes in liquefied soil are presented in Section 7.3.

The finite element method allows explicit consideration of the non-linear characteristics of pipe-soil interaction in both the transverse and longitudinal direction as well as non-linear stress-strain relations for pipe material. T. O'Rourke (1988), Suzuki et al. (1988) and Kobayashi et al (1989) as well as Liu and M. O'Rourke (1997b) have used the finite element approach to evaluate buried pipe response to spatially distributed transverse PGD. Assumptions and numerical results from each group are presented here.

T. O'Rourke

T. O'Rourke (1988) simulated the soil deformation by the beta probability density function given in Equation 7.1. Figure 7.3 shows the deformation of both the soil and the pipe.

As shown in Figure 7.3, L_a is the distance from the margin of the PGD zone to an assumed anchored point in the undisturbed soil beyond the PGD zone. The anchored point in the T. O'Rourke (1988) model was located where the bending strain is less than 1×10^{-5}.

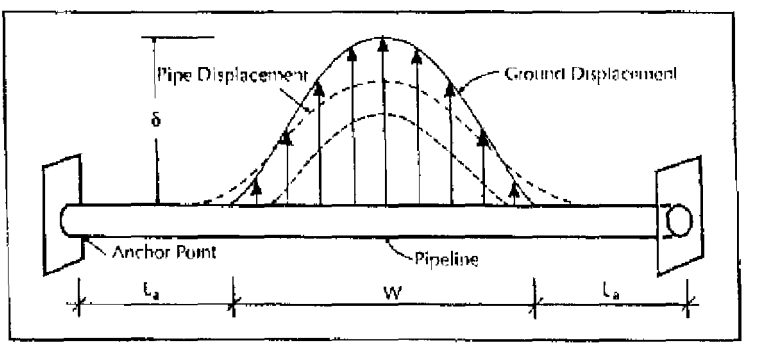

After T. O'Rourke, 1988

■ Figure 7.3 Parameters for T. O'Rourke's Model

Figure 7.4 presents the maximum tensile strain versus the maximum ground displacement for various widths of the PGD zone for an X-60 pipe with 0.61 m (24 in) diameter, 0.0095 m (3/8 in) wall

thickness and burial depth H = 1.5 m (5 ft). For the three widths considered, as shown in Figure 7.4, the width of 10 m (33 ft) results in the largest tensile strain in the pipe for any given value of δ.

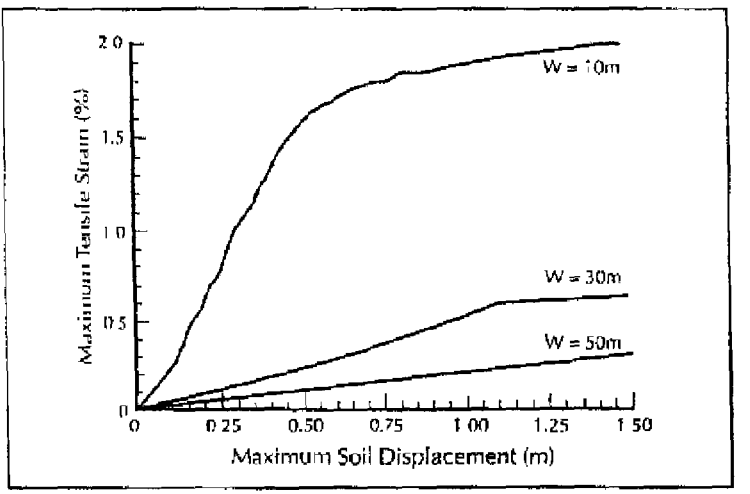

After T O Rourke, 1988

■ **Figure 7.4 Maximum Tensile Strain vs. Maximum Ground Displacement for Various Width of PGD Zone**

Figure 7.5 presents the maximum compressive strain as a function of δ for a width of 30 m. In this plot, the soil density ranged from 18.8 to 20.4 kN/m³ (115 to 122 pcf) and the soil friction angle ranged from 35° to 45°. Note there is no difference in pipe response for δ < 0.5 m (1.6 ft) and only a 30% difference for δ = 1.5 m (5 ft). Based on these observations, T. O'Rourke (1988) concluded that the width of the PGD zone has a greater influence on the magnitude of pipe strains than the soil properties.

From Figures 7.4 and 7.5, the peak tensile and compressive strains for a width of 30 m (98 ft) and δ = 1.5 m (5 ft) are about 0.61% and 0.32%, respectively. This indicates that the induced axial pipe strain at least in the T. O'Rourke (1988) model, is significant.

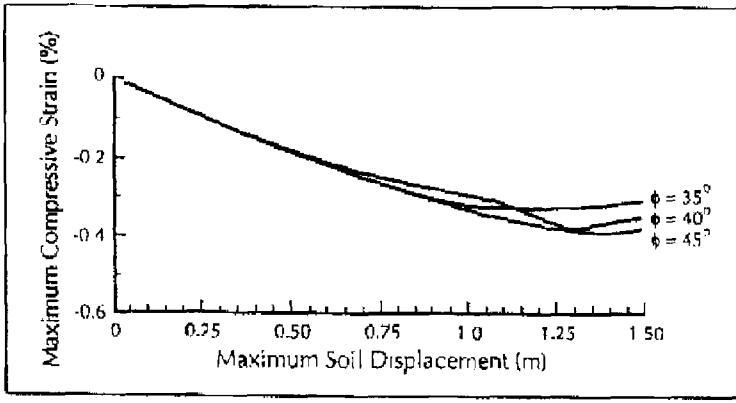

After T. O'Rourke, 1988

■ **Figure 7.5 Maximum Compressive Strains vs. Maximum Ground Displacement for Different Soil Friction Angles**

Suzuki et al.

Suzuki et al. (1988) expressed the pattern of transverse ground displacements by the cosine function raised to the n power as given in Equation 7.2. The normalized patterns for four values of n are shown in Figure 7.2. The patterns for n close to zero approximate abrupt transverse PGD while the patterns for $n \geq 1$ correspond to spatially distributed transverse PGD.

Suzuki et al.'s physical model is similar to T. O'Rourke's shown in Figure 7.3 except for the PGD pattern and the anchored length L_a. Suzuki et al. note that L_a needs be long enough such that the axial friction at the pipe-soil interface can fully accommodate the axial movement of the pipe due to the PGD. That is, there should be no flexural or axial strain in the pipe at the anchor points. It turns out that the anchored length in Suzuki et al.'s model is much larger than that in the T. O'Rourke (1988) model.

Figure 7.6 presents the influence of the width of the PGD zone on pipe strain for X-52 grade steel, 0.61 m (24 in) diameter, 0.0127 m (1/2 in) wall thickness and H = 1.5 m (5 ft). For given values of W and δ, the tensile and compressive strains are about equal. This suggests that the axial strain in the pipe is small. A certain width of the PGD zone somewhere around 30 m (98 ft) results in the largest pipe strain. Note that although the pipes are somewhat different, the tensile pipe strains in Figures 7.4 and 7.6 are similar for W = 30 and 50 m (164 ft).

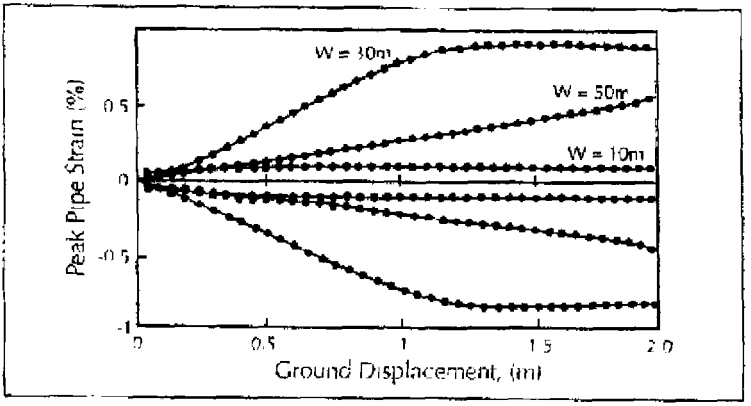

After Suzuki et al. 1988

■ Figure 7.6 Maximum Strain vs. PGD for Different Width of the PGD Zone; X-52 Grade Steel

Kobayashi et al.

Kobayashi et al. (1989) used the same shape function and followed the same procedure as Suzuki et al.'s to deal with the problem. They consider an X-42 grade steel pipe with 0.61 m (24 in) diameter and 0.0095 m (3/8 in) wall thickness. Kobayashi et al.'s results for the peak tensile strain are shown in Figure 7.7 for various of widths of the PGD zone. Note that the largest pipe strain occurs for a width of about 19 m (62 ft) in their model.

Liu and M. O'Rourke

Liu and M. O'Rourke (1997b) developed a finite element model, utilizing large deformation theory, non-linear pipe-soil interaction forces (soil springs) and Ramberg Osgood stress-strain relations for the pipe material. The pipe is modeled as a beam coupled by both axial and lateral soil springs. The anchor length of the pipe is long enough (up to 400 m (1312 ft)) such that both the flexural and axial pipe strain are essentially zero at the two anchor points. The pipe is assumed surrounded by loose to moderately dense sand (friction angle $\phi = 35°$ and soil density $\gamma = 1.87 \times 10^4$ N/m^3 (115 pcf)) with a burial depth $H_c = 1.2$ m (4 ft) from ground surface to the top of the pipe. The resulting elasto-plastic soil springs are based on the TCLEE Guideline (ASCE, 1984) and

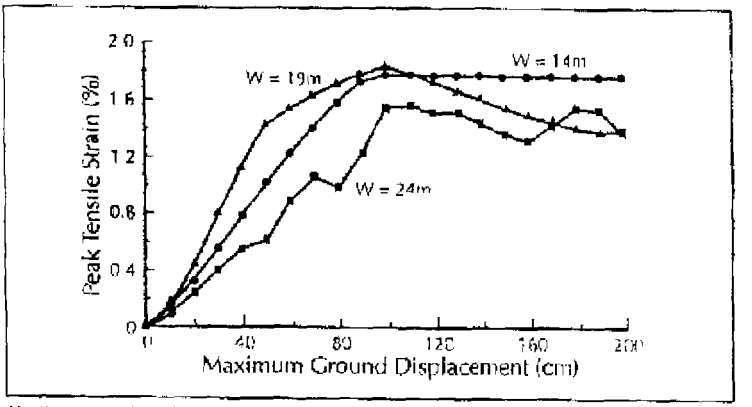

After Kobayashi et al., 1989

■ Figure 7.7 Peak Tensile Strain vs. Maximum Ground Displacement; X-42 Grade Steel

have peak transverse, p_u, and longitudinal, t_u, resistance of 1.0×10^5 and 2.4×10^4 N/m (571 and 137 lbs/in) respectively. The relative displacements between pipe and soil at which the peak transverse and longitudinal soil resistances are mobilizing are 0.06 and 3.8×10^{-3} (2.4 and 0.15 in), respectively.

Figure 7.8 shows the maximum tensile and compressive strains in the pipe versus the ground displacement for W = 10, 30 and 50 m, while Figure 7.9 shows the maximum pipe displacement versus the maximum ground displacement. Both these figures are for

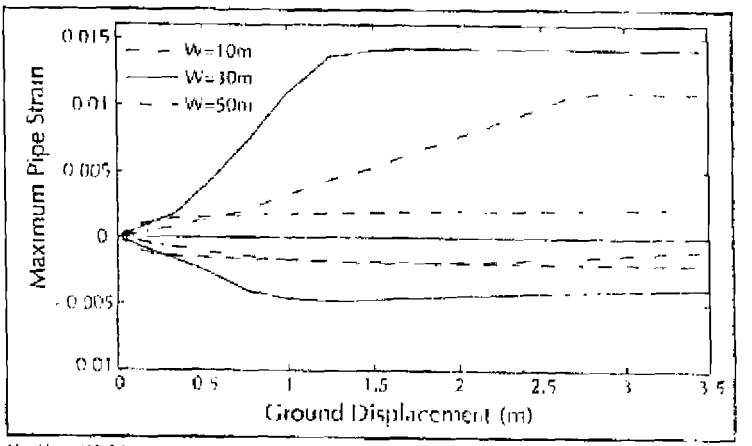

After Liu and M. O'Rourke, 1997b

■ Figure 7.8 Maximum Pipe Strain vs. Ground Deformation; X-52 Grade Steel

an X-52 grade steel pipe with D = 0.61 m (24 in), t = 0.0095 m (3/8 in) and the ground deformation pattern given in Equation 7.3. Except for W = 10 m, Figure 7.8 indicates that the peak tensile strain is substantially larger than the peak compressive strain, particularly for larger values of δ. Also, for the three widths considered, the pipe strains are largest for W = 30 m. Although the pipes are somewhat different, the peak tensile strains shown in Figure 7.8 match reasonably well with Suzuki et al.'s shown in Figure 7.6 for all three widths. Also, both the peak tensile and compressive strains match reasonably well with the T. O'Rourke (1988) results for W = 30 and 50 m.

As shown in Figure 7.9, the maximum pipe displacement more or less matches the ground deformation up to a certain critical displacement δ_{cr}. Thereafter, the pipe strain remains relatively constant while the pipe displacement increases more slowly with ground deformation. For ground deformation greater than δ_{cr}, the pipe bending strain varies slightly (increasing for small widths and decreasing for large widths) and axial strain increases slowly, which results in the maximum tensile strain remaining more or less constant.

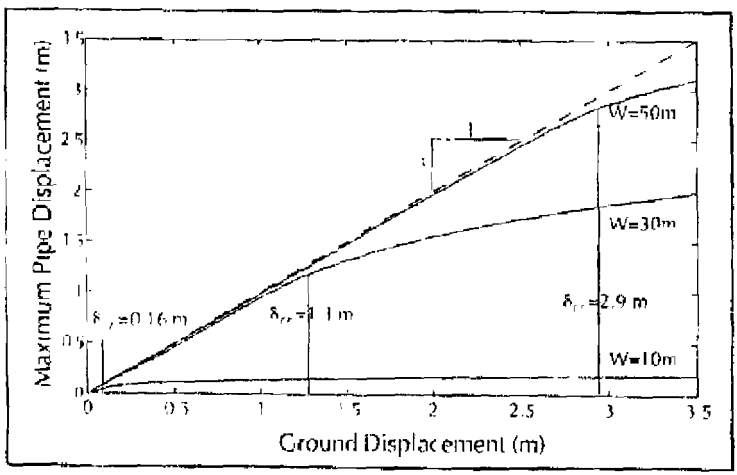

After Liu and M. O'Rourke, 1997b

■ Figure 7.9 Maximum Pipe Displacement vs. Ground Displacement; X-52 Grade Steel

For a fixed value of the width of the PGD zone (W = 30 m), Figure 7.10 shows the spatial distribution of pipe and soil displacement for $\delta = 0.5\delta_{cr}$, δ_{cr} and $2\delta_{cr}$.

Note that the pipe deformation matches fairly well with the ground deformation over the whole width of the PGD zone for $\delta \leq \delta_{cr}$. However, for $\delta > \delta_{cr}$, the maximum pipe displacement is less than the maximum ground displacement (from Figure 7.10, 40% less for $\delta = 2\delta_{cr}$), and "width" of the deformed pipe (i.e., length over which the pipe has noticeable transverse displacement) is larger than the width of the PGD zone. As a result, the curvature of the pipe is substantially less than the curvature of the ground for $\delta > \delta_{cr}$. As shown in Figure 7.10 for W = 30 m, the pipe curvature at $\delta = 2\delta_{cr}$ is comparable to the pipe curvature at $\delta = \delta_{cr}$.

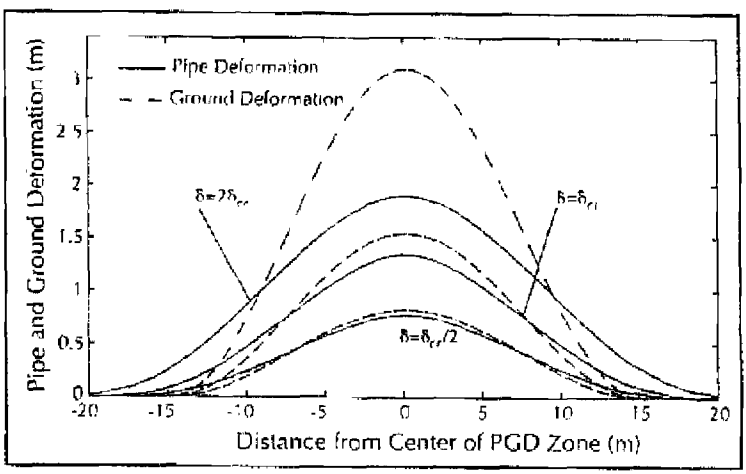

After Liu and M. O'Rourke, 1997b

■ Figure 7.10 Pipe and Ground Deformation for W = 30 m; X-52 Grade Steel

Figures 7.11 and 7.12 show the distribution of bending moments and axial forces in the pipe at $\delta = \delta_{cr}$ for W = 10, 30 and 50 m. As one might expect, the bending moments in Figure 7.11 are symmetric with respect to the center of the PGD zone and similar to those for a laterally loaded beam with built-in (i.e., fixed) supports near the margins of the PGD zone. That is, there are positive moments near the center of the PGD zone and negative moments

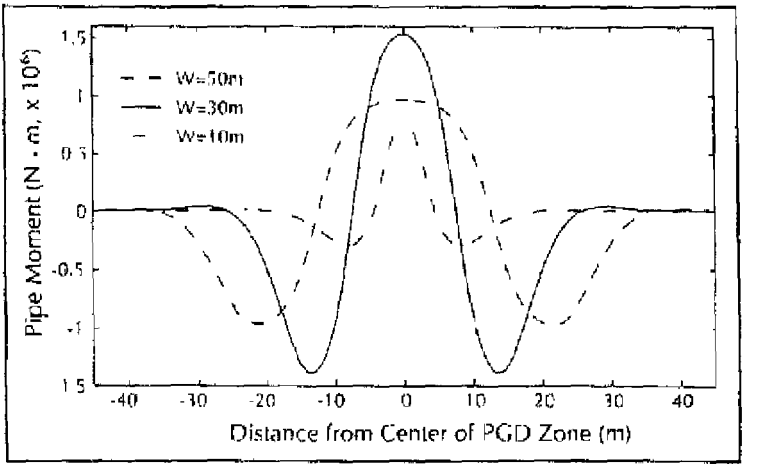

After Liu and M. O'Rourke, 1997b

■ Figure 7.11 Distribution of Bending Moment for Three Widths ($\delta = \delta_{ar}$)

near the margins. The moments vanish roughly 10 m beyond the margins. Note that the bending moments for $W = 30$ m are larger than those for $W = 10$ m or 50 m.

The axial forces in the pipe shown in Figure 7.12 are, as expected, also symmetric about the center of the PGD zone. The axial forces are maximum near the center of the zone and decrease in a fairly linear fashion with increasing distance from the center of the zone. Unlike the moments, the axial forces become small only at substantial distances beyond the margins of the zone (note the different distance scales in Figures 7.11 and 7.12). Also, for the three widths considered, the axial force was an increasing function of the width of the PGD zone (i.e., largest for $W = 50$ m and smallest for $W = 10$ m).

The transverse loading on the pipe also results in axial movement of the pipe, that is, inward movement towards the center of the PGD zone. This inward movement is an increasing function of the ground movement δ as shown in Figure 7.13. For $\delta = 4$ m (13 ft), this inward movement at the margins of the PGD zone for the pipe under consideration was 0.002, 0.07 and 0.15 m (0.08, 2.8 and 5.9 in) respectively for $W = 10$, 30 and 50 m.

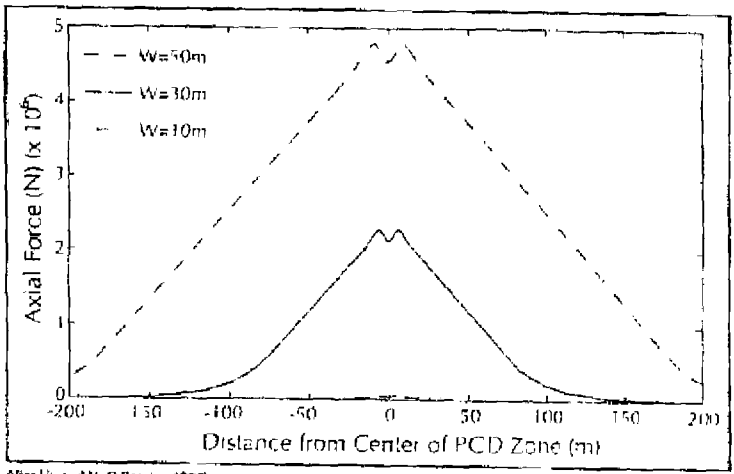

After Lie and M. O Rourke, 1997b

■ Figure 7.12 Distribution of Axial Force for Three Widths ($\delta = \delta_{pl}$)

The influence of other parameters upon the pipe behavior was also determined and is shown in Figures 7.14 through 7.20. Unless otherwise indicated, these results are for W = 30 m, X-52 grade steel, D = 0.61 m (24 in), t = 0.0095 m (3/8 in), p_o = 1.0×10

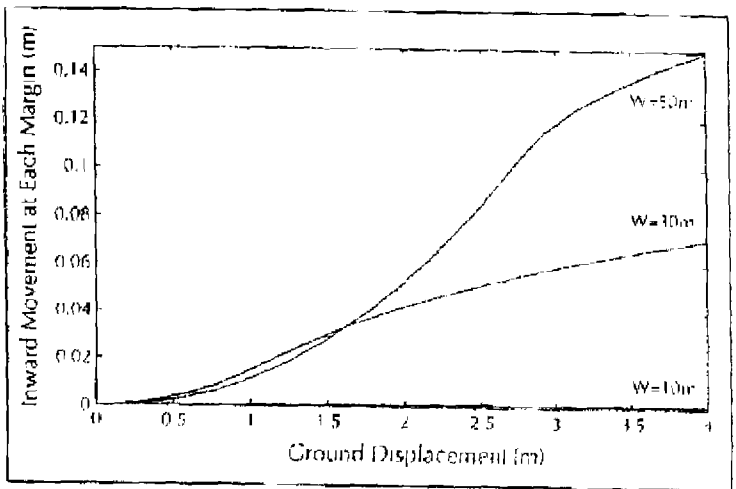

■ Figure 7.13 Pipe Inward Movement at Each Margin of PGD Zone

N/m, (571 lbs/in), $t_s = 2.4 \times 10^4$ N/m (137 lbs/in) and the M. O'Rourke (1989) pattern of ground deformation. Figure 7.14 shows, for example, the influence of diameter on peak tensile and compressive strains. Note that both the peak tensile and compressive strains are increasing functions of diameter.

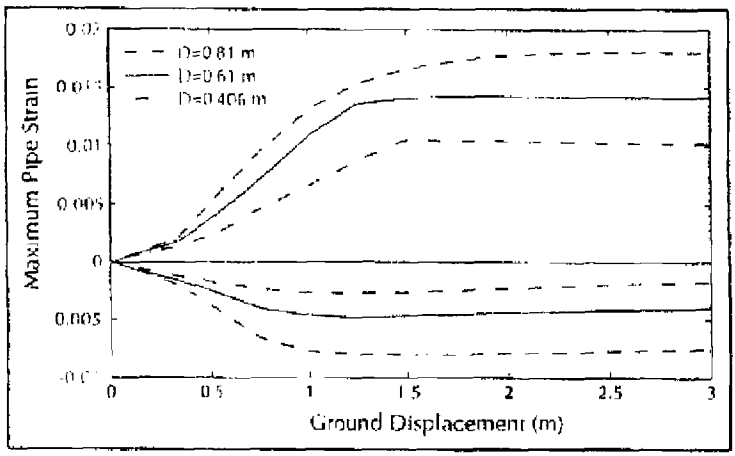

After Liu and M. O'Rourke, 1997b

■ Figure 7.14 Influence of Pipe Diameter, D

For the pipe model considered the peak tensile strain is, to a greater or lesser extent, a function of all the parameters shown in Figures 7.14 through 7.20. However, the peak compressive strain is essentially independent of the wall thickness, as shown in Figure 7.15, and the steel grade, as shown in Figure 7.18.

The peak tensile strain is an increasing function of the pipe diameter and the transverse (lateral) soil spring resistance. It is a decreasing function of the pipe wall thickness, the steel grade and to a lesser extent the longitudinal (axial) soil spring resistance.

In terms of anchor length L_a, a zero anchor length resulted in substantially larger pipe strain than L_a = 15 m (49 ft) or 400 m (1312 ft) as shown in Figure 7.19.

With reference to the PGD pattern, the M. O'Rourke (1989) pattern (same as the Suzuki et al. pattern with $n = 2$) resulted in the largest pipe strain for $W \geq 30$ m as shown in Figure 7.20. However, the Suzuki et al. (1988) pattern with $n = 1$ resulted in the largest strain for $W \leq 10$ m.

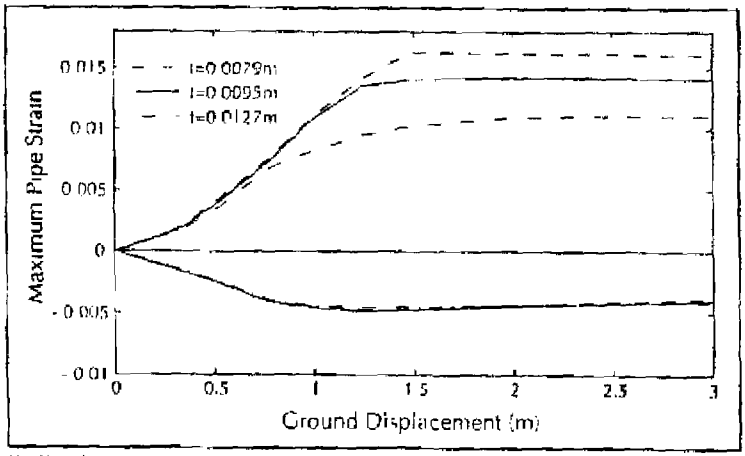

After Liu and M. O'Rourke, 1997b

■ Figure 7.15 Influence of Wall Thickness, t

The parameter which most strongly influences the tensile strain is the width of the PGD zone, followed by the transverse soil spring resistance, pipe diameter, steel grade, wall thickness, PGD pattern, anchor length of the pipe and longitudinal soil spring

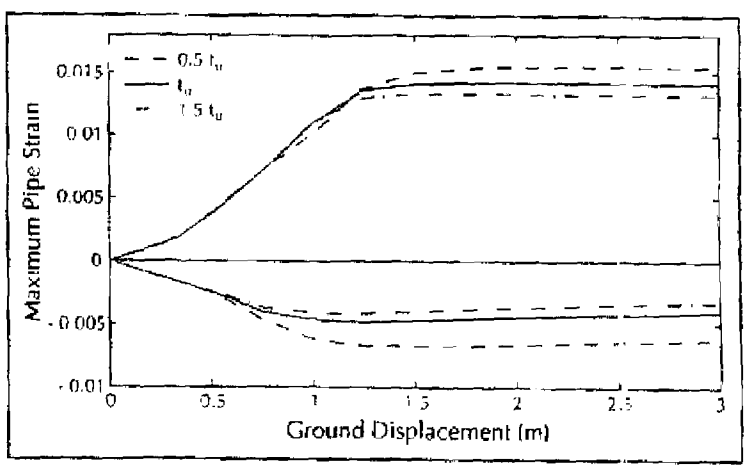

After Liu and M. O Rourke, 1997b

■ Figure 7.16 Influence of Peak Longitudinal Soil Resistance, t_u

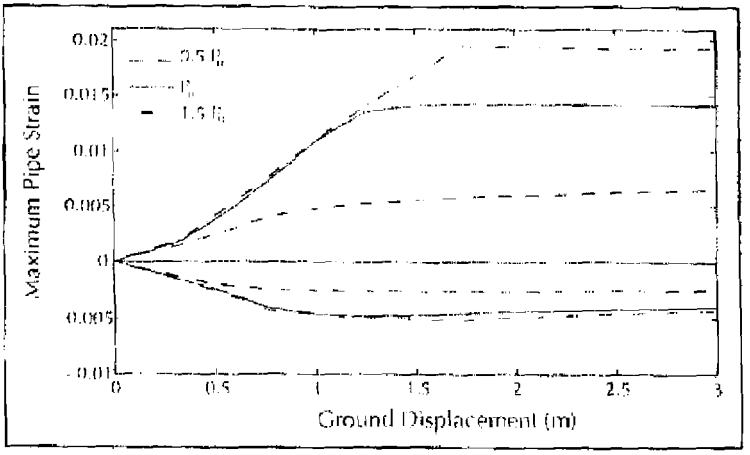

After Liu and M. O'Rourke, 1997b

■ Figure 7.17 Influence of Peak Transverse Soil Resistance, p_u

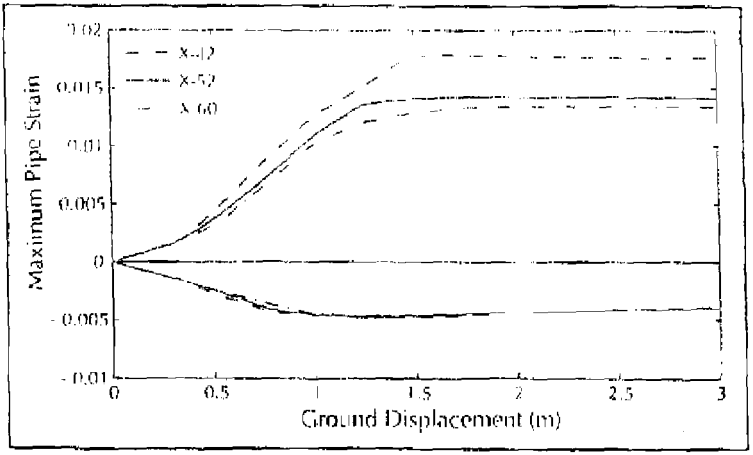

■ Figure 7.18 Maximum Pipe Strain for Three X-Grade Steel Materials

resistance. The critical ground displacement δ_{cr} was found to be an increasing function of width of the PGD zone and the lateral pipe-soil interaction force, but a decreasing function of steel grade, pipe diameter, axial pipe-soil interaction force and pipe wall thickness.

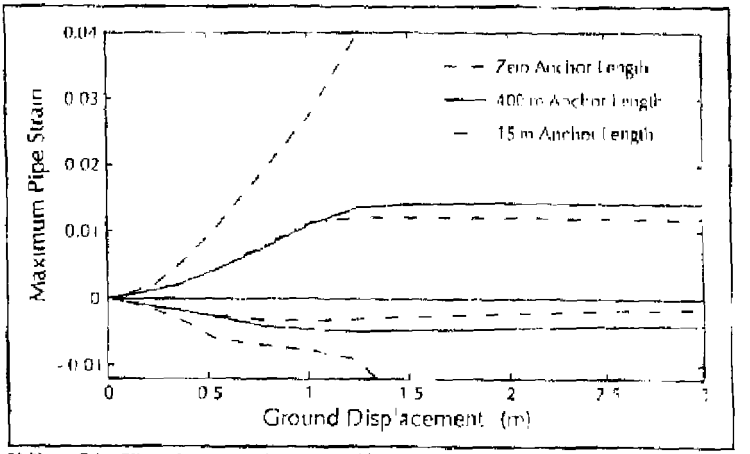

■ Figure 7.19 Effect of Anchored Length Outside of PGD Zone L_x

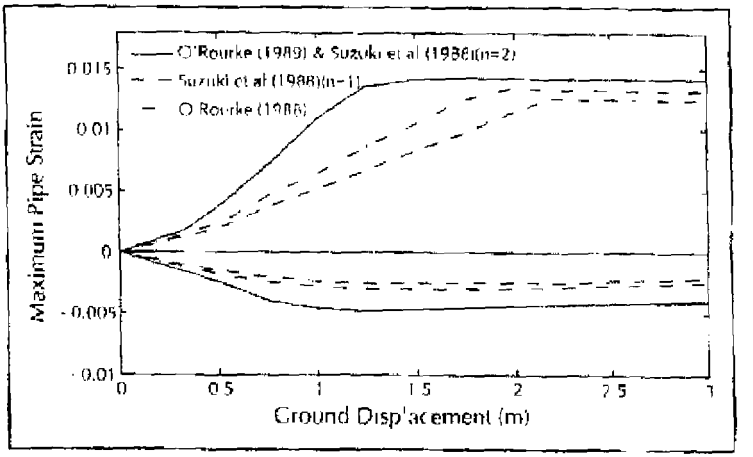

■ Figure 7.20 Effect of Spatially Distributed PGD Patterns

Miyajima and Kitaura

Miyajima and Kitaura (1989) model a pipe subject to spatially distributed transverse PGD as a beam on an elastic foundation as shown in Figure 7.21. The equilibrium equations for the pipe are expressed as follows

$$EI\frac{d^4y_1}{dx^4} + K_1 y_1 = K_1\delta\left(1-\sin\frac{\pi x}{W}\right) \qquad \left(0 < x < \frac{W}{2}\right) \qquad (7.4)$$

$$EI\frac{d^4y_2}{dx^4} + K_2 y_2 = 0 \qquad \left(x \geq \frac{W}{2}\right) \qquad (7.5)$$

where y_1 and y_2 are the transverse pipe displacement in and outside the PGD zone, K_1 and K_2 are the equivalent lateral soil spring coefficient in and outside the PGD zone, and EI is the flexural rigidity of the pipe cross-section. The equivalent soil springs K_1 and K_2 are based upon recommended practice in Japan (Japan Gas Association, 1982) in which non-linear characteristics are taken into consideration.

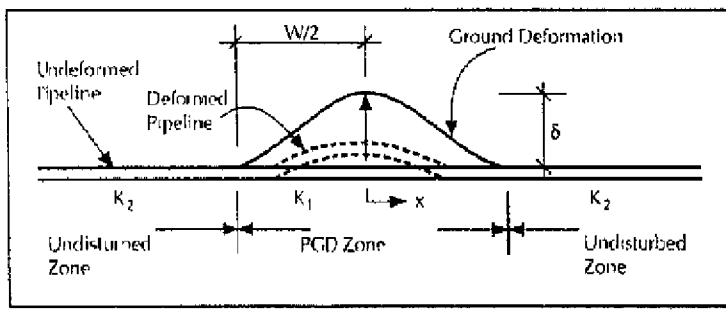

After Miyajima and Kitaura 1989

■ Figure 7.21 Analytical Model for Pipeline Subject to Spatially Distributed Transverse PGD

Miyajima and Kitaura's equations provide a clear mechanical model and are solved by using a modified transfer matrix method. The maximum bending stress for a 16 inch (40 cm) diameter and

1/4 inch (0 6 cm) wall thickness steel pipe in a competent soil layer above the liquefied layer (i.e., $K_1 = K_2$) is shown in Figure 7 22 as a function of the width of the PGD zone W for three values of ground deformation δ.

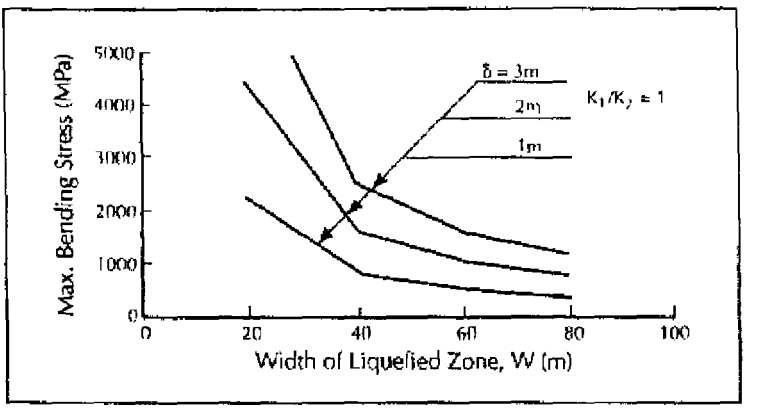

After Miyajima and Kitaura 1989

■ Figure 7 22 Maximum Bending Stress vs Width of PGD Zone for Three Values of Ground Deformation

As one might expect intuitively, the pipe stress is an increasing function of the ground deformation δ. For a given value of δ, the stress is a decreasing function of W for the range of widths considered by Miyajima and Kitaura. Note that they used small deformation flexural theory, which does not account for axial strain due to arc-length effects.

M. O'Rourke

M. O'Rourke (1989) developed a simple analytical model for pipeline response to spatially distributed transverse PGD. He considered two types of response as shown in Figure 7.23. For a wide width of the PGD zone, the pipeline is relatively flexible and its lateral displacement is assumed to closely match that of the soil. For this case, the pipe strain was assumed to be mainly due to the ground curvature (i.e., displacement controlled). For a narrow width, the pipeline is relatively stiff and the pipe lateral displace-

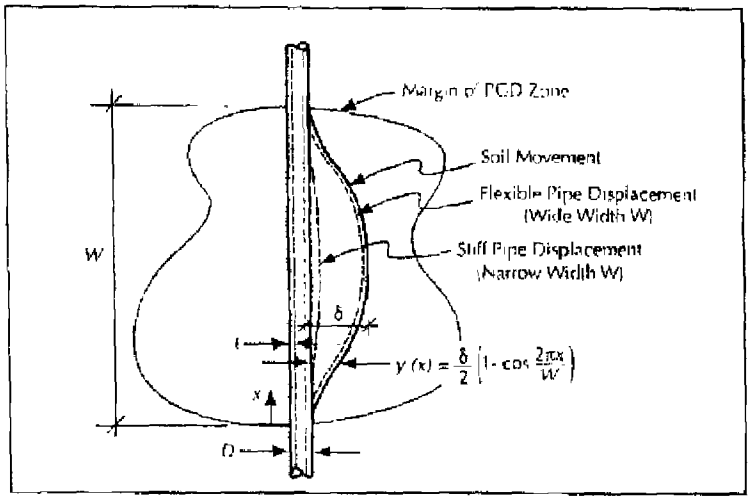

After M. O'Rourke, 1989

■ Figure 7.23 M. O'Rourke's Analytical Model for Pipeline Subject to Spatially Distributed Transverse PGD

ment is substantially less than that of the soil. In this case, the pipe strain was assumed to be due to loading at the soil-pipe interface (i.e., loading controlled).

For the wide PGD width/flexible pipe case, the pipe is assumed to match the soil deformation given by Equation 7.3. The maximum bending strain, ε_b, in the pipe, is given by:

$$\varepsilon_b = \pm \frac{\pi^2 \delta D}{W^2} \tag{7.6}$$

In this simple model, the axial tensile strain is based solely upon the arc-length of the pipe between the PGD zone margins. Assuming the pipe matches exactly the lateral soil displacement, the average axial tensile strain, ε_a, is approximated by:

$$\varepsilon_a = \left(\frac{\pi}{2}\right)^2 \left(\frac{\delta}{W}\right)^2 \tag{7.7}$$

For the narrow width/stiff pipe case, the pipe is modeled as a beam, built-in at each margin (i.e., fixed-fixed beam), subject to the maximum lateral force per unit length p_u at the soil-pipe interface. For this case the axial tension due to arc-length effects is small and neglected. Hence, the maximum strain in the pipe is given by:

$$\varepsilon_h = \pm \frac{p_u W^2}{3\pi E t D^2} \tag{7.8}$$

Note that M. O'Rourke (1989) assumes that the pipe is fixed at the margins and hence neglects any inward (i.e., axial) movement of pipe at the margin of PGD zone. As a result, Equation 7.7 overestimates the axial strain in the pipe, as will be shown later.

Liu and M. O'Rourke

Based on the Finite Element results described previously, Liu and M. O'Rourke (1997b) found that pipe strain is an increasing function of ground displacement for ground displacement less than a certain value, δ_{cr}, and pipe strain does not change appreciably thereafter. For example, for $W = 30$ m, as shown in Figure 7.8, the maximum tensile strain is an increasing function of maximum soil displacement up to a value of $\delta = 1.3$ m (4.3 ft). For larger values of δ, the maximum tensile strain remains at a relatively constant value of roughly 0.014. Similar behavior is observed for other widths.

In reality, the pipe resistance to transverse PGD is due to a combination of flexural stiffness and axial stiffness. The analytical relations developed below are for an elastic pipe. Although the inelastic pipe case is more complex, the elastic relations provide a basis for interpreting finite element results and, as will be shown later, are directly applicable to transverse PGD case histories from Niigata.

For small widths of the PGD zone, the critical ground deformation and pipe behavior are controlled by bending. The mechanism is the same as that in the M. O'Rourke (1989) model for the stiff pipe case (i.e., two end fixed beam with constant distributed load). The critical ground deformation is given by:

$$\delta_{\text{cr - beam}} = \frac{5p_u W^4}{384EI} \qquad (7.9)$$

For very large widths of the PGD zone, the pipe behaves like a flexible cable (i.e., negligible flexural stiffness). For this case, the critical displacement is controlled primarily by the axial force. For a parabolic cable shown in Figure 7.24, the relation between the axial force T at the ends and the maximum lateral deformation (or sag) δ is:

$$T = \frac{p_u W^2}{8\delta} \qquad (7.10)$$

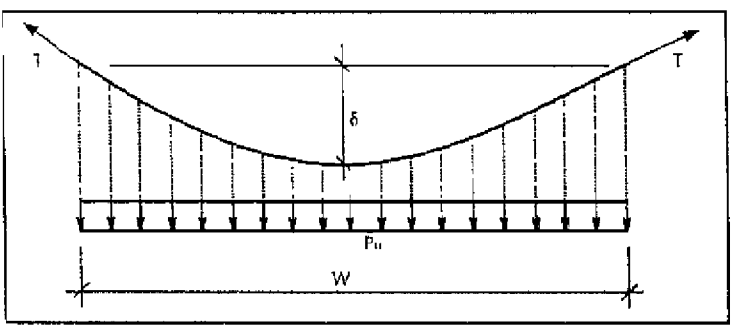

■ Figure 7.24 Flexible Cable System

As shown in Figure 7.10, the ground displacement is larger than the pipe displacement in the middle region of the PGD zone (assumed herein to be $W/2$), over which the maximum transverse resistance per unit length, p_u, at the pipe-soil interface (i.e., the distributed load) is imposed. Taking the "sag" over this middle region to be $\delta/2$, the interrelationship between the tensile force, T, and ground displacement, δ, is given by:

$$T = \pi Dt\sigma = \frac{p_u (W/2)^2}{8(\delta/2)} = \frac{p_u W^2}{16\delta} \qquad (7.11)$$

where σ is the axial stress in the pipe (assumed to be constant within the PGD zone).

Inward movement of the pipe occurs at the margin of the PGD zone due to this axial force. Assuming a constant longitudinal friction force, t_u, beyond the margins, the pipe inward movement at each margin is:

$$\Delta_{inward} = \frac{\pi D t \sigma^2}{2Et_u} \tag{7.12}$$

The total axial elongation of the pipe within the PGD zone is approximated by the average axial strain given by Equation 7.7 (i.e., arc-length effect) times the width W. This elongation is due to stretching within the zone ($\sigma W/E$) and inward movement at the margins from Equation 7.12. That is,

$$\frac{\pi^2 \delta^2}{4W} = \frac{\sigma W}{E} + 2 \cdot \frac{\pi D t \sigma^2}{2Et_u} \tag{7.13}$$

The critical ground deformation, $\delta_{cr\,axial}$ for "cable-like" behavior and the corresponding axial pipe stress, σ, can be calculated by simultaneous solution of Equations 7.11 and 7.13. These values are presented in Table 7.1 for three values of the width W and the standard properties mentioned previously (i.e., D = 0.61 m, t = 0.0095 m, p_u = 1.0×10^5 N/m, t_u =2.4×10^4 N/m). Note that the critical ground deformation is controlled by axial force for this case, and that the maximum axial stress at $\delta = \delta_{cr}$ is an increasing function of width of the PGD zone.

■ Table 7.1 Critical Ground Displacements and Stresses for "Cable-Like" Elastic Pipe

Item	W = 10 m	W = 30 m	W = 50 m
$\delta_{cr\,axial}$ (Equations 7.11 and 7.13)	0.37 m	1.5 m	2.85 m
σ (Equations 7.11 and 7.13)	92.8 MPa	206 MPa	301 MPa

For any arbitrary width of the PGD zone, somewhat between small and very large, resistance is provided by both flexural (beam) and axial (cable) effects. Considering these elements to be acting in parallel,

$$\delta_{cr} = \frac{1}{\frac{1}{\delta_{cr-bending}} + \frac{1}{\delta_{cr-axial}}} \qquad (7\ 14)$$

Table 7 2 lists the resulting critical displacements of an elastic pipe (D = 0 61 m, t = 0 0095 m, etc) for W = 10, 30 and 50 m along with the corresponding elastic finite element results For W = 30 and 50 m, the critical displacement from Equation 7 14 matches that from the elastic finite element model. However, for W = 10 m, the critical displacement from Equation 7.14 is an order of magnitude less than that from the elastic finite element model This is due, in part, to the assumption of a constant transverse load p_u on the pipe for bending effects in the simplified approach. The finite element model, on the other hand, uses transverse elasto-plastic soil springs As noted previously, one obtains the full load p_u from the soil spring only after 0.06 m (2.4 in) of the relative transverse displacement between the pipe and the soil Hence, although the fully loaded pipe deflects in bending only 0.015 m (0.6 in) for W = 10 m, the bases of the soil springs must move an additional 0.05 m (2.4 in) to obtain the full transverse resistance p_u

■ Table 7.2 Critical Ground Displacements for Elastic Pipe

Item	W = 10 m	W = 30 m	W = 50 m
$\delta_{cr-bending}$ (Equation 7.9)	0.015 m	1.22 m	9.6 m
$\delta_{cr-axial}$ (Table 7.1)	0.37 m	1.5 m	2.85 m
δ_{cr} (Equation 7.14)	0.015 m	0.67 m	2.2 m
δ_{cr} (FE Approach)	0.16 m	0.70 m	2.1 m

Note that the critical displacements for both the simplified elastic and elastic finite element models in Table 7 2 underestimate δ_u for an inelastic pipe shown for example in Figure 7.8. This is due to the fact that for the inelastic pipe model, the steel modulus decreases after yielding, and the pipe must undergo larger deformations such that the strain energy in the pipe equals the work done by the distributed soil springs.

The maximum strains in an elastic pipe are due to the combined effects of axial tension (cable behavior) and flexure (beam behavior), and can be expressed as:

$$\varepsilon_{elastic} = \begin{cases} \dfrac{\pi\delta}{2}\sqrt{\dfrac{t_u}{AEW}} \pm \dfrac{\pi^2\delta D}{W^2} & \delta \le \delta_{cr} \\ \dfrac{\pi\delta_{cr}}{2}\sqrt{\dfrac{t_u}{AEW}} \pm \dfrac{\pi^2\delta_{cr} D}{W^2} & \delta > \delta_{cr} \end{cases} \qquad (7\ 15)$$

where A is the pipe cross-sectional area.

7.2.3 Comparison Among Approaches

Table 7.3 presents a summary of the pipe properties and the pipe-soil interaction forces used in the approaches mentioned above

■ Table 7.3 List of Parameters in Seven Approaches

Item	M. O'Rourke (1989)	Miyajima & Kitaura (1989)	T. O'Rourke (1988)	Suzuki et al. (1988)	Kobayashi et al. (1989)	Liu & O'Rourke (1997b)
Method	Analytical	Analytical	F.E	F.E	F.E	Both
Diameter (m)	0.50, 1.01	0.406	0.61	0.61	0.61	0.61
Thickness	0.0127, 0.0063	0.006	0.0095	0.0127	0.0095	0.0095
Material	Mild steel	Elastic	X-60	X-52	X-42	X-52
t_u (N/m)	-	-	2.4×10^5	1.9×10^5	1.9×10^5	2.4×10^5
P_u (N/m)	8.7×10^4	-	7.7×10^5	1.5×10^5	1.15×10^5	1.0×10^5

Comparing the approaches is difficult since the models have different diameters, wall thickness, pipe-soil interaction parameters, etc. Nevertheless, the bending strains can be compared since the analytical relation for bending strain given in Equation 7.15 suggest that it is only a function of δ, D and W.

Figure 7.25 shows the pipe bending strain for $W > 20$ m, backcalculated from the different approaches, plotted as a function of $\delta D/W$. Herein the bending strain is calculated as one half of the sum of the tensile and compressive pipe strains. Note that the Kobayashi et al. (1989) approach is not included since they did not present compressive strain. In this figure, the straight line with a slope of π^2 is the analytical relation given in Equation 7.6. Note that the Suzuki et al. (1988) as well as the Liu and M. O'Rourke (1997b) results both match the analytical relation fairly well. The T. O'Rourke (1988) results are somewhat less than the analytical results while the Miyajima and Kitaura (1989) results are somewhat higher.

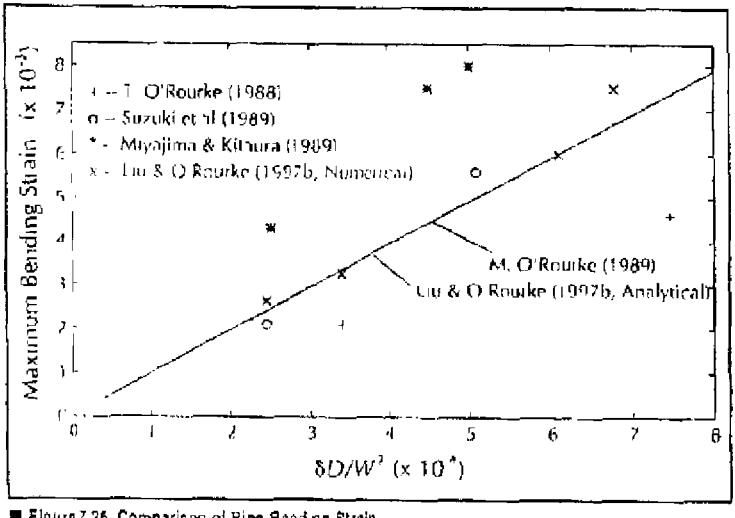

■ Figure 7.25 Comparison of Pipe Bending Strain

Another type of comparison involves the general trends in results from the various approaches. For example, the Liu and M. O'Rourke (1997b) results suggest that axial effects are important in that the tensile strains are larger than the compressive strains. This agrees with the numerical results by T. O'Rourke (1988). In addition, for the three widths considered, the tensile strains are largest for $W = 30$ m which agrees with the numerical results by Suzuki et al. (1988). However, the Liu and M. O'Rourke (1997b) numerical results described above differ from those by T. O'Rourke

(1988), specifically for the width of the PGD zone W = 10 m. Similarly, the Liu and M. O'Rourke (1997b) numerical results differ from those by Suzuki et al. (1988) in that the tensile pipe strains are significantly larger than the compressive strains. It is believed that this difference is due to the comparatively heavy wall thickness used in the Suzuki et al. (1988) model (note as shown in Figure 7.15 that a heavier wall thickness reduces the peak tensile strain but essentially has no effect on the peak compressive strain) in combination with a relatively weak longitudinal soil spring.

7.2.4 Comparison with Case Histories

The performance of buried pipelines subject to the transverse PGD during the 1971 San Fernando earthquake provides case histories to test the approaches described above. In the case history shown in Figure 2.11(a), a water transmission pipeline (Pipeline 2) made of Grade-C steel with 1370 mm (54 inch) diameter and 7.9 mm (5/16 inch) wall thickness was subjected to spatially distributed transverse PGD with the maximum ground displacement δ of 0.7 m (2.0 ft.) and a width W of about 400 m (1312 ft.). From Equation 7.6, the bending strain in the pipe with W = 400 m and δ = 0.7 m (2.3 ft) would be 6.0×10^{-5} while the axial tension strain would be 7.6×10^{-6} and the critical displacement δ_{cr} is over 10 m (33 ft). Hence, the maximum tension strain is 6.8×10^{-5} while the net compression strain is 5.2×10^{-5}. Since these values are below the tensile rupture and local buckling strain respectively for the pipe, one expects the pipe would not be damaged by this transverse PGD. The expected behavior matches the observed behavior in that there was no failure within the PGD zone. Note, however, that one break was observed at a location close to but outside the PGD zone, where the pipeline was connected to a ball valve by a mechanical joint at a reinforced concrete vault. According to T. O'Rourke and Tawfik (1983), the mechanical joint was severely deformed and showed signs of repeated impacts. This evidence of repeated impacts suggests that the damage may have been due to wave propagation as opposed to PGD effects.

Although there has been a fair amount of research activity directed at the problem of buried pipe subject to distributed transverse PGD, case histories of continuous pipeline failure due solely to distributed transverse PGD appears fairly unusual.

7.2.5 Expected Response

Although the approximate method (Liu and M. O'Rourke, 1997b) described above is strictly applicable to elastic pipe and widths of 30 m or greater, they prove useful for many realistic design situations. Suzuki and Masuda (1991) present values for the width W and the amount of movement δ, for transverse PGD observed in the Niigata Japan after the 1964 event. Based on roughly 40 separate sites, the amount of ground movement δ ranged from about 0.3 m to 2.0 m, while the width of the PGD zone W ranged from about 100 m to 600 m.

For $W \geq 100$ m (328 ft), steel pipe with $D = 0.61$ m (24 in), $t = 0.0095$ m (3/8 in), the critical ground deformation from Equation 7.14 is 6.0 m (20 ft) or more, which is much larger than the maximum observed ground displacement of 2.0 m (6.6 ft). Also the estimated peak tensile (i.e., combined axial and flexural) strain for $\delta = 2$ m from Equation 7.15 is less than the yield strain for X-grade steel but slightly above the yield strain for GR-B grade steel. Hence, an X-grade pipe behaves elastically and the strain can be estimated by Equation 7.15.

The maximum pipe strains are shown in Figure 7.26 as a function of the ground deformation using both the simplified analytical and numerical models by Liu and M. O'Rourke (1997b). The finite element results for both X-grade and GR-B grade steels are identical for δ less than about 1.6 m. At that location there is a kink in the GR-B curve, indicating the onset of inelastic behavior in that material. Note that the analytical model (i.e., Equation 7.15) results compare favorably with the finite element values.

The approximate analytical approach does overestimate to some degree the peak tensile strain and underestimates the peak compressive strain. This suggests that the estimated axial strains are somewhat too large. However, the differences are relatively small, particularly in light of the accuracy of geotechnical predictions for expected value of the spatial extent and ground movement of PGD zones.

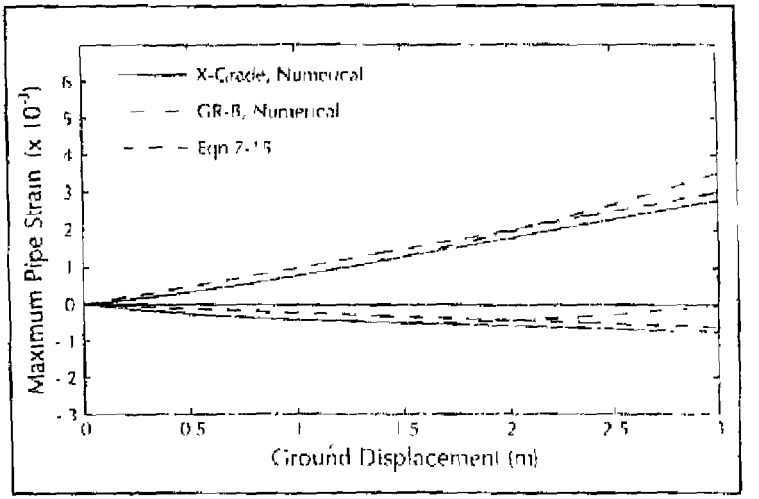

After Liu and M. O'Rourke, 1997b

■ Figure 7.26 Maximum Pipe Strain vs. Ground Displacement for W = 100 m

7.3 Pipelines in Liquefied Soil

As mentioned previously, the top of the liquefied soil layer is commonly located below the bottom of the pipe. However, when the pipe is buried in saturated sand such as at a river bed, or in a sea bed, the soil surrounding the pipe may liquefy during strong seismic shaking. In this case, the pipe may deform laterally following the flow of liquefied soil down a gentle slope, or move upward due to buoyancy, especially when a manhole is present or a compressive load acts on the pipe. For example, according to Suzuki et al. (1988) and Takada (1991), a sewage pipe with manhole and a gas pipe (150 mm in diameter) were uplifted out of the ground due to buoyancy in combination with a compressive load caused by longitudinal permanent ground deformation during the 1964 Niigata earthquake. A compressive load can also be induced by temperature change and/or internal operating pressure in a pipe restrained against longitudinal expansion.

7.3.1 HORIZONTAL MOVEMENT

When a pipeline is surrounded by liquefied soil, the pipe may move laterally due to the flow of liquefied soil downslope. Using the same model as shown in Figure 7.3, Suzuki et al. (1988) studied the response of a buried pipe, surrounded by liquefied soil, subject to spatially distributed transverse PGD. The presence of the liquefied soil was modeled by assuming that the lateral soil coefficient (K_1) for a pipe surrounded by liquefied soil is some fraction of the corresponding value (K_2) for competent, non-liquefied soil. Figure 7.27 shows the peak pipe strain as a function of the amount of PGD, δ, for three values of the reduction factor. For this plot, the width of the PGD zone is 30 m, while the pipe properties are the same as that listed in Table 7.3 for the Suzuki et al. approach.

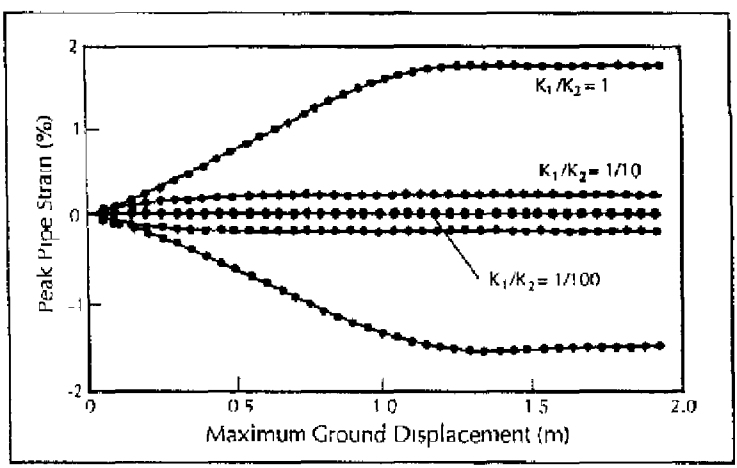

After Suzuki et al. 1988

■ Figure 7.27 Maximum Strain vs. δ for Three Soil Spring Constants

As one might expect, the peak pipe strain for competent non-liquefied soil (i.e., $K_1/K_2 = 1$, also see Figure 7.6 for $W = 30$ m) is in all cases larger than that for liquefied soil. As a rough approximation, the pipe strain for $\delta \geq 1.5$ m (5 ft) is proportional to the soil coefficient reduction factor.

As noted in Section 5.3, the equivalent soil spring coefficient for liquefied soil, according to Takada et al (1987), ranges from 1/1000 to 1/3000 of that for non-liquefied soil, while other scholars suggest that the ratio is from 1/100 to 5/100. Hence, for the same amount of PGD and width of the PGD zone, a pipe surrounded by liquefied soil is much less likely to be damaged by spatially disturbed transverse PGD. Hence, for design purpose, it seems reasonable to conservatively assume that a pipe subject to spatially distributed transverse PGD is located in a competent non-liquefied soil which overlays the liquefied layer.

7.3.2 Vertical Movement

If the soil immediately surrounding a buried pipe liquefies, the pipe may uplift due to the buoyancy. A few studies have been done regarding this uplifting response. Takada et al. (1987) conducted a series of laboratory tests and estimated the liquefied soil spring constant by combining the test values with analytical solutions. Yeh and Wang (1985) analyzed the dynamic (i.e., seismic shaking and buoyancy effects) pipe response by using a simplified beam-column model for the pipe. They concluded that the dynamic displacement is relatively small (less than 20% of static pipe displacement due to the buoyancy) when the surrounding soil is liquefied.

Using 2 cm (0.8 in) diameter polyethylene pipeline, Cai et al. (1992) carried out a series of laboratory tests and observed pipe response due to soil liquefaction. Figure 7.28 shows the two system models. The model in Figure 7.28 (a) is a pipeline without a manhole while (b) is for a pipeline with a manhole. In both models, the end of the pipe can be either fixed, elastically constrained, or free. The model pipe is 1.2 m (4 ft) in length, which would correspond to a prototype length of 50 m (164 ft) for a prototype diameter of 83 cm (32 in). In these tests, only the shaking and uplifting response can be observed since the simulated ground surface before and after liquefaction is normally flat. That is, lateral response of the pipe is not modeled. For an elastically restrained case, they found that the dynamic strain due to shaking is less than 10% of the static strain due to uplifting and hence can be neglected when estimating the maximum uplifting strain in the pipe. When a manhole and/or an axial compressive force are introduced,

the upward response is larger. For elastically constrained ends, the pipe keeps uplifting till a portion of pipe near the center of PGD zone is at the ground surface. However, when a non-liquefied soil layer (60 mm in thickness) is used as cover, the pipe came to rest at the interface of the non-liquefied and liquefied layers.

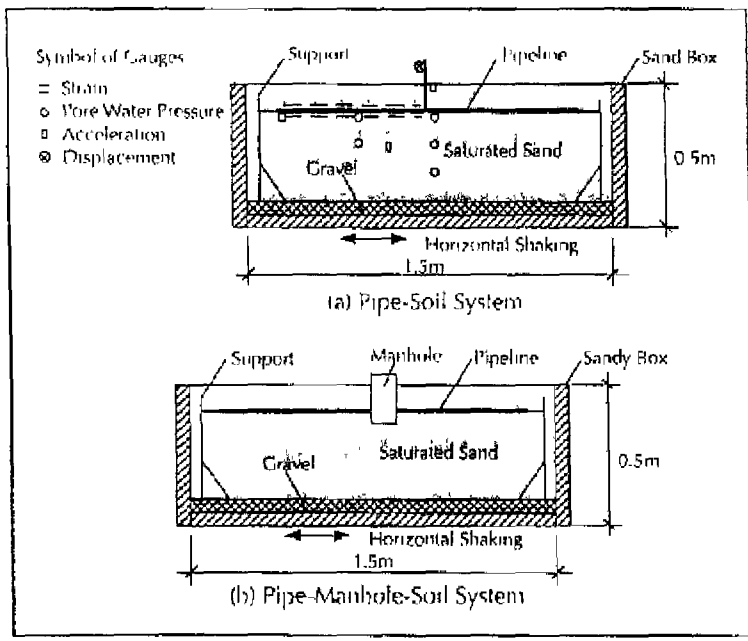

After Cai et al., 1992

■ Figure 7.28 Model System of Buried Pipeline in Liquefied Soil

Hou et al. (1990) analyzed the pipe strain due to buoyancy effects by a finite element approach. In the analysis, the non-linearity of both steel material and interaction force at the pipe-soil interface outside the liquefied zone are considered. The uplifting force per unit length, P_{uplift}, acting on the pipe within the liquefied zone, can be expressed as

$$P_{uplift} = \frac{1}{4}\pi D^2(\gamma_{soil} - \gamma_{contents}) - \pi D t \gamma_{pipe} \qquad (7.16)$$

where γ_{soil}, γ_{pipe}, $\gamma_{contents}$ are the weights per unit volume of lique-

fied soil, pipe and pipe contents (i.e., water, gas, etc.) respectively. Note that the uplifting force will decrease when a portion of the pipe is at the ground surface.

The pipe is constrained beyond the margins of the liquefied zone by restraint due to the non-liquefied soil. That is, the behavior is similar to a beam, built in at each margin, subject to a uniform upward load. The maximum strain in a steel pipe is shown in Figure 7.29 as a function of the length of the liquefied zone for $\gamma_{soil} = 2.0\times10^4$ N/m^3,(120 pcf), $\gamma_{contents} = 0.8\times10^4$ N/m^3 (48 pcf), $t = 0.0079$ m (0.31 in) and three separate pipe diameters. Note that the initial stress ($\sigma_{initial} = 180$ MPa) is due to internal operating pressure and/or temperature change.

As shown in Figure 7.29, the maximum pipe strain occurs at a certain width of the liquefied zone, W_{cr}. For the width less than W_{cr}, the pipe strain is an increasing function of the width, while the pipe strain decreases with the increasing width thereafter. The critical width can be estimated by setting Equation 7.8 equal to Equation 7.6 with $\delta = H_c$ (depth from the ground surface to the top of the pipe). That is:

$$W_{cr} = \sqrt[4]{\frac{3\pi^3 EtH_c D^3}{p_0}} \qquad (7.17)$$

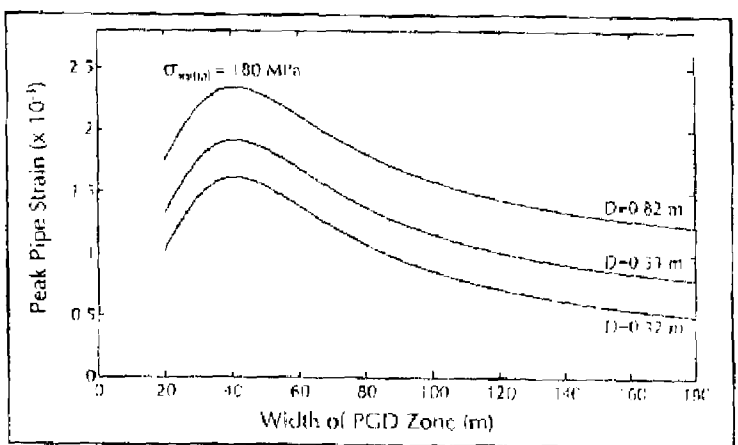

After Hou et al. 1990

■ Figure 7.29 Maximum Strain vs. Width of the Liquefied Zone

For H_c = 1.2 m (4 ft), D = 0.61 m (24 in) and p_u = 1.0×10⁴ N/m (57 lbs/in), the estimated critical width of the liquefied zone from Equation 7.17 is 47 m (154 ft), which is slightly larger than the observed critical width of about 42 m (138 ft) in Figure 7.29.

In fact, the buoyancy per unit length given in Equation 7.16 is about 10% of the lateral pipe-soil interaction for a pipe surrounded by non-liquefied soil. That is, it is equivalent to the curve K_1/K_2 = 1/10 in Figure 7.27. A comparison of Figures 7.27 and 7.29 indicates that the Suzuki et al.'s results match Hou et al. (1990) reasonably well. That is, for $W \geq 30$ m and D = 0.61 m (24 in) in Figure 7.27, the peak pipe strain is about 0.2% while for D = 0.53 m (21 in) in Figure 7.29, the peak pipe strain is 0.19%. Since the maximum strain is less than both critical strain of tensile failure and local buckling, the pipe is unlikely to be damaged due to the buoyancy although it may uplift out of the ground when the width of the liquefied zone is large. For situations where a large uplifting displacement is not desirable (for example for submarine pipelines), the following equation derived from the principle of conservation of energy can be used to determine the maximum uplift displacement and/or the spacing for piles or other pipe restraints.

$$\delta_{max}^{4} + \frac{16I}{A}\delta_{max} - \frac{16p_u W_s^4}{AE\pi^2} = 0 \qquad (7.18)$$

where A is the cross-section area, and W_s is the spacing of the piles as shown in Figure 7.30.

The peak pipe strain is then given by:

$$\varepsilon_{max} = \pm\frac{\pi^2\delta_{max}D}{W_s^2} + \frac{\pi^2\delta_{max}^2}{4W_s^2} \qquad (7.19)$$

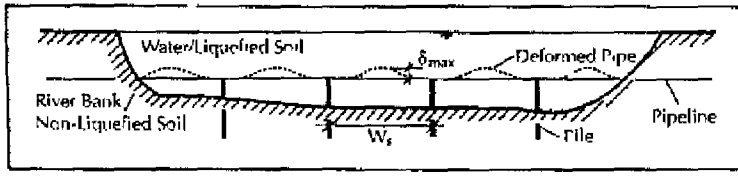

■ Figure 7.30 Profile of Pipeline Crossing Liquefied Zone

7.4 LOCALIZED ABRUPT PGD

Two patterns of transverse PGD are shown in Figure 7.1. The spatially distributed pattern in Figure 7.1(a) has been discussed extensively above. In relation to the localized abrupt pattern shown in Figure 7.1(b), it was noted that this corresponds more or less to a pair of fault offsets provided that the PGD zone is sufficiently wide. Hence, a key question involves determining the minimum width of the PGD zone, above which the fault crossing models discussed in more detail in Chapter 8 are applicable. Recall that data gathered by Suzuki and Masuda (1991) and shown in Figure 2.8 suggest that PGD zone widths are typically larger than 80 m. Herein a width of 50 m is considered. Figure 7.31 shows the bending moment and axial force in a continuous buried pipeline subjected to a localized abrupt pattern of transverse PGD. The amount of ground movement δ = 1.0 m (3.3 ft) while the width of the PGD zone, W, is 50 m. The pipe and soil properties are D = 0.61 m (24 in), t = 0.0095 m (3/8 in), $\gamma_{soil} = 1.8 \times 10^4$ N/m^3, $\phi = 35°$.

Note that the bending moment is essentially zero over a distance of roughly 20 m (66 ft) near the center of the PGD zone. Hence, in terms of flexure, the continuous pipe behaves as if it was subject to two separate fault offsets, both having a pipe-fault angle of 90°, with no interaction between them. The pipe axial force near the center depends on the width of the PGD zone. It would be zero if the width is large enough such that all the axial force is provided by the friction at the pipe-soil interface within the PGD zone. In this case, the pipe behavior (both tension and flexure) due to a localized abrupt pattern of transverse PGD is the same as that for a pipe crossing a fault with intersection angle of